Ch. 4: Characterization Studies

****

Characterization studies of the as prepared blend polymer electrolyte specimens and cathode materials done by using X-ray diffraction, differential scanning calorimetry, scanning electron microscopy and Fourier transform infrared spectroscopy are explained thoroughly in this chapter. Ionic transport number measurements of these blend specimens are further carried out.

****

4.1 Introduction

The characterization studies of the as prepared PVA-PEO blend specimens and cathode material have been carried out using the following characterization techniques described briefly as follows.

♣ ***X-Ray Diffraction***

X-ray diffraction (XRD) is one of the most powerful techniques that provide an essential insight regarding structure of polymer (especially of a semicrystalline polymer) nature of polymer, types and degree (amount) of the crystalline and amorphous phases present in a polymer, etc. This study also informs about the complexation as well as the miscibility and compatibility amongst the host polymers and other constituents in case of blend polymer electrolyte systems [1,2]. In the present study, to obtain all such information about polymer electrolyte specimens, including the cathode material ($LiMn_2O_4$), their respective XRD spectra along with those of the pure constituents are measured in the '2θ' range of 10° to 70° and thoroughly investigated using *'Shimadzu Diffractometer'* and *'Bruker Powder XRD Model D2 Phaser'*, XRD instruments respectively.

♣ ***Differential Scanning Calorimetry***

One of the most important techniques which throws light on the thermal parameters such as glass transition temperature, crystallization temperature and melting temperature of the polymeric specimens is 'Differential Scanning Calorimetry (DSC)'. Usually, when an amorphous or a glassy solid is heated, the DSC thermogram shows a presence of exothermic and endothermic peaks. Such peaks usually arise when a solid amorphous phase transforms to a crystalline phase and melting state thereafter [3]. Usually, before melting temperature, there can be an endothermic peak, generally known as *'Glass Transition'*. But if the specimen is a glass, it may show an exothermic peak at which the amorphous phase converts into

crystalline phase. The last endothermic peak refers to the melting temperature 'T_m' and indicates the transition from crystalline to amorphous phase. Similar phenomenon is likely to occur in case of polymer also wherein this endothermic peak arises due to the melting process of polymer and is termed as *'Melting Peak'*. In addition to the melting temperatures, the degree of crystallinity 'X_c' also plays a major role in obtaining information regarding thermal properties of the blend polymeric specimens as it explains the extent to which the crystalline phase is present in that particular polymeric specimen. Hence, in order to obtain a thorough insight regarding the thermal behaviour of the as prepared blend specimens, their melting temperature 'T_m' and degree of crystallinity 'X_c' are thoroughly investigated where 'X_c' values are calculated using the following equation:

$$X_c = \frac{\Delta H_m}{\Delta H_m^0} \times 100\% \qquad \ldots\ldots\ldots\ldots\ldots (4.1)$$

where, ΔH_m = heat of fusion of the individual blend specimens and ΔH_m^0 = equilibrium heat of fusion of pure PEO = 203 J/g [4,5]. This way of evaluating the degree of crystallinity of the polymer electrolytes from the recrystallized enthalpy (ΔH_m) is quite common [6]. Melting temperature (T_m) is taken at the apex of melting endotherm (an endothermic transition upon heating wherein, crystalline solid melts to liquid state) and is the temperature at which the crystalline/semicrystalline solid phases of the pure polymers melt to the liquid amorphous phases [3,7,8]. The DSC thermograms of pure PEO polymer and the present polymeric blend specimens are depicted from 30 °C to 75 °C using *'SII EXSTAR 6000'* and *'DSC822^e Mettler Toledo'* DSC instruments respectively, except for the pure PVA polymer whose DSC scan is depicted from 30 °C to 230 °C.

♣ ***Scanning Electron Microscopy***

The surface morphological observation is one of the most important elements of study of any material and this can be successfully investigated by using 'Scanning Electron

Microscopy' (SEM) technique [9]. Moreover, this technique detects the phase separation interface [10]. Hence, to obtain an overview regarding the surface of blend polymeric specimens, their SEM micrographs are thoroughly inspected at the constant magnification of 100 X and resolution of 100 μm using *'JEOL JSM-5610LV'* scanning electron microscope.

♣ ***Fourier Transform Infrared Spectroscopy***

Fourier Transform Infrared (FT-IR) Spectroscopy is one of the most exquisite tools to identify molecular components as well as structures on the basis of infrared absorption bands, especially in case of polymeric specimens. The FT-IR spectra of various materials obtained by infrared spectroscopy measures various vibrational energy levels in infrared region, usually in the range of 4000 cm^{-1} to 400 cm^{-1}. The vibrational energy levels corresponding to the respective molecules of the sample are observed in the form of sharp peaks and broad bands. The chemical interactions and complexation occurring amongst various constituents forming the test specimen, result in the (i) shifting and/or broadening of bands, (ii) appearance/disappearance of bands/peaks and (iii) variation in the intensity of the peaks. When a polymer film is exposed to infrared radiations, the polymer molecules selectively absorb specific wavelength. This causes the change in dipole moment of these molecules owing to which vibrational energy levels of the molecule transfer from ground state to excited state. The frequency is determined by vibrational energy gap. In the present study, the FT-IR measurements of pure constituents and blend polymer electrolytes are carried out from 4000 cm^{-1} to 500 cm^{-1} and of $LiMn_2O_4$ powder from 4000 cm^{-1} to 375 cm^{-1} using *'FT-IR 4100 JASCO Model'* FT-IR instrument.

♣ ***Transport Number Measurement***

The transport number of an electrolyte material is one of the most important criteria to be studied as it informs about the dominating species participating in the process of

conduction. This *'Transport Number'* of an ion in an electrolyte solution is defined as *'the fraction of total electrical current carried in that solution by that particular ion'* [11]. Usually, the 'ionic' transport number for ionic species in case of an ideal electrolyte should be unity whereas; it should be zero for the electronic species. The continuous efforts are done in order to prepare solid electrolytes which satisfy this criterion of an ideal electrolyte. In the present research work, the transport number measurements of the polymeric electrolytes are carried out in order to obtain an insight regarding the type of dominating species (ions/electrons) that participate in the process of conduction [12].

4.2 Characterization Studies of Pure Constituents

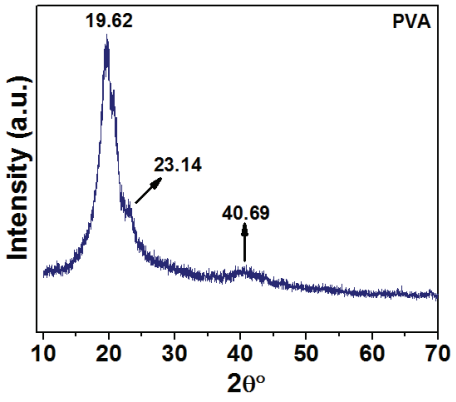

Fig. 4.1 XRD scan of pure PVA

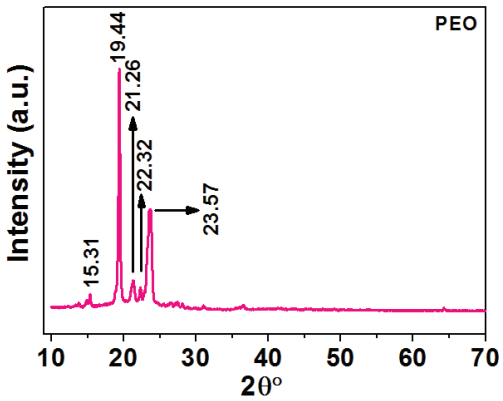

Fig. 4.2 XRD scan of pure PEO

The XRD scans of pure PVA and PEO polymers are as shown in Figs. 4.1 and 4.2, respectively. As observed from Fig. 4.1, the XRD scan of pure PVA depicts an intense and broad peak at ~ 19°, a small kink at ~ 23° and a broad hump at ~ 40° whereas; the XRD spectrum of pure PEO as shown in Fig. 4.2, shows the presence of small kink at ~ 15°, ~ 21° and ~ 22° as well as two sharp and intense peaks at ~ 19° and ~ 23°, respectively. The peaks at ~ 19° and ~ 23° confirm the crystalline nature of PEO polymer where, the presence of the crystalline phase of PEO is due to the ordering of the polyether side chains [13-20].

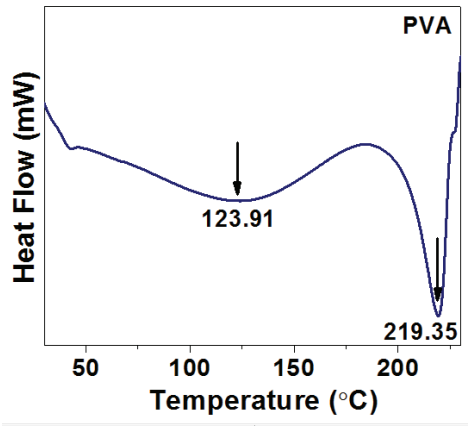

Fig. 4.3 DSC scan of pure PVA

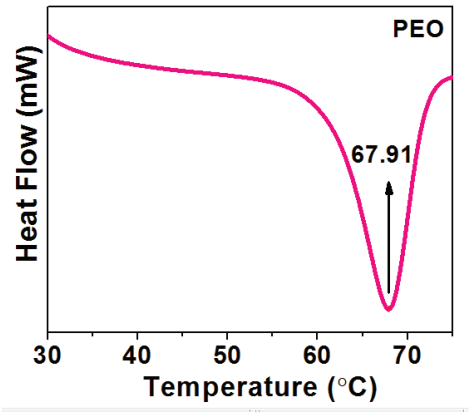

Fig. 4.4 DSC scan of pure PEO

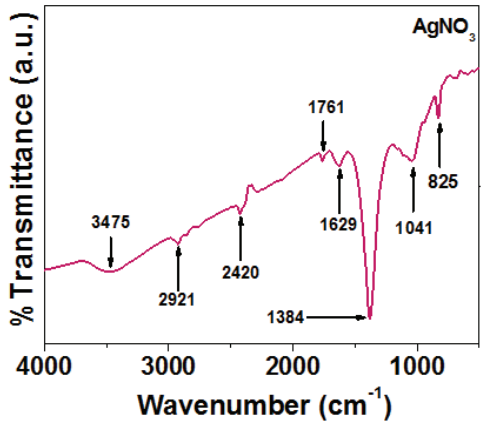

Fig. 4.5 FT-IR spectrum of $AgNO_3$

Table 4.1 Vibrational modes & wavenumbers exhibited by $AgNO_3$

Wavenumber (cm^{-1})	Assignment
3475	-----
2921	-----
2420	-----
1761	-----
1629	-----
1384	Characteristic of NO_3^- in the free form.

1041	-----
825	O-N Sretching of nitrate group.

Table 4.2 Vibrational modes & wavenumbers exhibited by $LiCF_3SO_3$

Wavenumber (cm^{-1})	Assignment
3490	-----
1638	-----
1264	$\nu_{as}(SO_3)$
1181	$\nu_{as}(CF_3)$
1033	$\nu_s(SO_3)$
776	$\delta_s(CF_3)$
644	$\delta_s(SO_3)$
578	$\delta_{as}(CF_3)$
	where,
	ρ = rocking, ν = stretching,
	δ = bending, as = asymmetric,
	s = symmetric

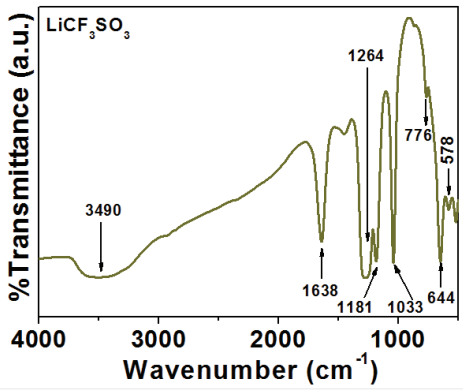

Fig. 4.6 FT-IR spectrum of $LiCF_3SO_3$

Table 4.3 Vibrational modes & wavenumbers exhibited by PEG

Wavenumber (cm^{-1})	Assignment
3520-3330	OH Stretching
2880	Stretching vibration of CH_2
1465	Bending vibration of CH_2/ C-O Stretching
1350	C-O Stretching
1260	C-O-C Ether Linkage
1110	C-C Stretching
947	CH_2 Rocking/
842	C-C Stretching

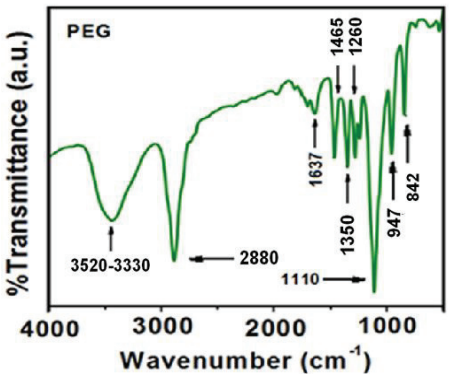

Fig. 4.7 FT-IR spectrum of PEG

Table 4.4 Vibrational modes & wavenumbers exhibited by EC

Wavenumber (cm^{-1})	Assignment
1808	C=O Stretching
1480	CH_2 Bending
1392	CH_2 Wagging
1168	C-O-C Symmetric
1076	Ring Breathing Mode
975	Skeletal Stretching
894	Ring Breathing Mode
775	CH_2 Rocking
716	C=O Bending

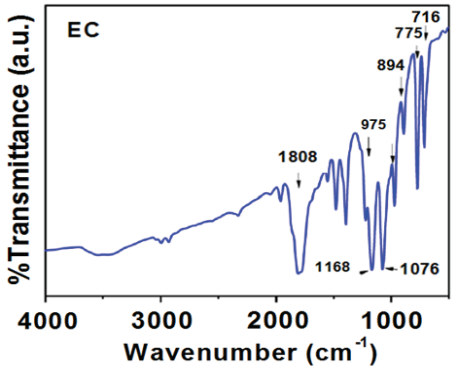

Fig. 4.8 FT-IR Spectrum of EC

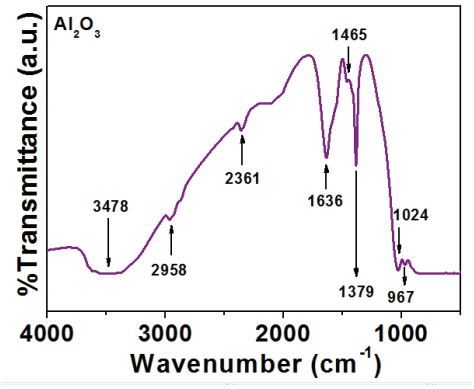

Fig. 4.9 FT-IR spectrum of Al_2O_3

DSC scans of pure PVA and pure PEO polymers are depicted in Figs. 4.3 and 4.4, respectively. Fig. 4.3 depicting the DSC thermogram of pure PVA shows the presence of a broad endothermic peak at ~ 123 °C and an endothermic peak at ~ 219 °C. The first peak appearing at ~ 123 °C corresponds to the glass transition temperature (T_g) whereas, the

second peak at ~ 219 °C refers to the melting temperature (T_m) of pure PVA. On the other hand, the DSC thermogram of pure PEO as depicted in Fig. 4.4 shows presence of a single endothermic peak at ~ 67 °C [21]. As pure PEO melts at this temperature, the temperature is said to be its melting temperature.

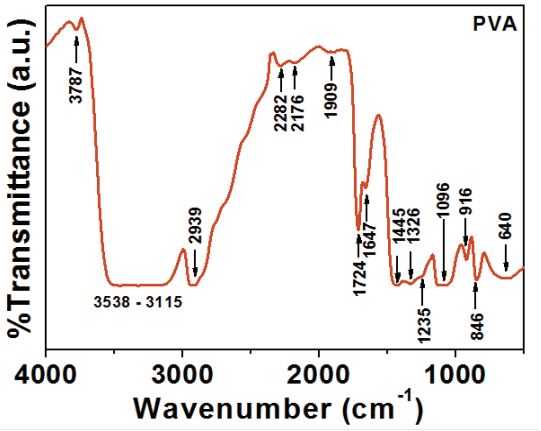

Fig. 4.10 FT-IR spectrum of PVA

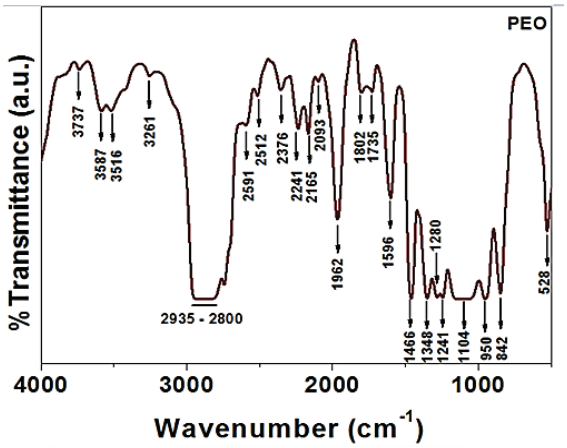

Fig. 4.11 FT-IR spectrum of PEO

Table 4.5 Vibrational modes & wavenumbers exhibited by PVA

Wavenumber (cm^{-1})	Assignment
3538-3115	Intermolecular OH Stretching (hydroxyl) band: characteristic feature of alcohols.
2939	C-H Stretching of CH_2
1724	C=O Stretching
1647	C=C Stretching
1445	CH_2 Scissoring/ CH Bending of CH_2
1326	CH_2 out of plane Bending/C-OH Plane Bending
1235	C-C Stretching/ C-H Wagging
1096	C–O Stretching/C-O-C Stretching/OH Bending
916	Skeletal
846	C-C Stretching
640	OH Twisting

Table 4.6 Vibrational modes & wavenumbers exhibited by PEO

Wavenumber (cm^{-1})	Assignment
3800-2700	Asymmetric C–H Stretching
2935-2800	C–H Stretching
2376	C=C Stretching
2241	C–H Stretching/ C=O Combination
2165	Asymmetric C–H Stretching/ C–H Deformation Combination
1962	Asymmetric Stretching Band
1735	C=O Stretching
1596	C=C Stretching
1466	CH_2 Scissoring
1348	CH_2 Wagging
1280	Asymmetric CH_2 Twisting
1241	Asymmetric CH_2 Twisting
1104	C-O-C Stretching
950	CH_2 Symmetric Rocking/ C–O–C Stretching
842	CH_2 Twisting /CH_2 Wagging
528	C–O–C Bending

The FT-IR spectra of $AgNO_3$ salt, $LiCF_3SO_3$ salt, PEG plasticizer, EC plasticizer, Al_2O_3 nano-filler, PVA polymer and PEO polymer are shown from Figs. 4.5 to 4.11,

respectively. Also, the band assignments for all these pure constituents have been listed in the respective tables from Tables 4.1 to 4.6 [4,7,22-44].

4.3 $[PVA_{(100-x)} : PEO_{(x)}] - 5$ wt% $AgNO_3 - 10$ wt% PEG (where, x = 10 % to 50 %) (PPAP) Series

The characteristic study of the blend specimens of a newly prepared novel PPAP series given as '$[PVA_{(100-x)} : PEO_{(x)}] - 5$ wt% $AgNO_3 - 10$ wt% PEG' is being studied in this part of the chapter. In the preparation of blends of this series, 'x' is varied from 10 % to 50 %. The changes occurring in various characteristic properties are investigated thoroughly for the gradually increasing concentration of PEO polymer and the simultaneously reducing amount of PVA polymer in the blends. XRD scan of each blend specimen of PPAP series is depicted in Fig. 4.12.

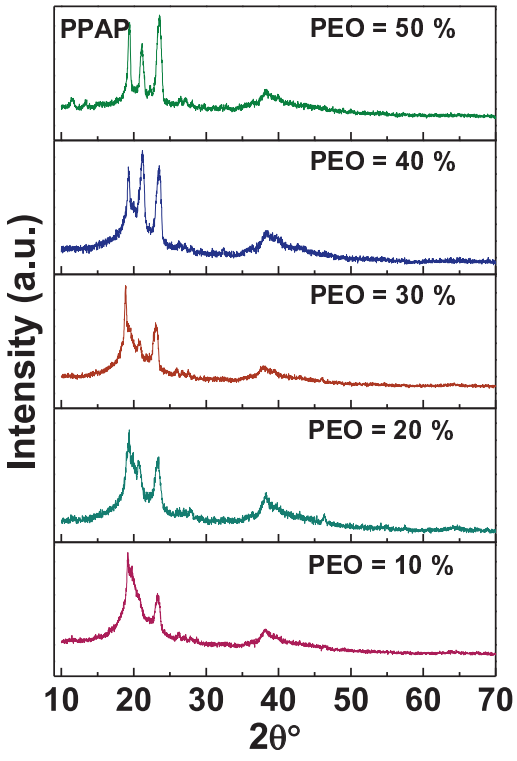

Fig. 4.12 XRD scans of blend specimens of PPAP series for varying PEO amounts

For the blend with 10 % of PEO, XRD scan shows presence of a broad peak at ~ 19° which resembles to semicrystalline nature of PVA polymer wherein, crystalline nature arises from the intermolecular interaction between PVA backbone chains via hydrogen bond [45]. With further addition of PEO in the blends upto 30 %, the peak gets prominently well-separated to form two intense peaks at 2θ ~ 19° and ~ 21°, respectively which can be attributed to the monoclinic crystal structure of PEO [46] and suggests the presence of crystalline nature of PEO which occur due to ordering of polyether side chains [19]. These peaks get intense and sharp with further addition of PEO in the blends.

Such a phenomenon suggests a good miscibility of both PVA and PEO polymers to make a best blend at PVA:PEO = 50:50. Along with the features of PEO, XRD scans show a consistent presence of a broad hump at ~ 40° of pure PVA. The presence of the features of both PVA as well as PEO host polymers in the XRD scan of each blend specimen of PPAP series points on some complexation and interaction occurring amongst the blend constituents. This suggests that compatibility and miscibility amongst host polymers of the blends gradually improves with substantial addition of PEO therein [1,47]. Also, the blending of PEO polymer with PVA retains the crystalline as well as the amorphous phases of the blend matrix. The reduction in the intensities of the observed peaks in each XRD scan of the blend specimen as compared to those with pure polymers suggests the substantial reduction in the degree of crystallinity upon blending of PVA with PEO. **Sengwa et al.** [48] also studied and discussed the same in PEO-PMMA blend electrolyte systems. **Hodge et al.** [49] explained the correlation amongst the degree of crystallinity and intensity of peaks. Further, the absence of peaks corresponding to the silver salt ($AgNO_3$) in the present case indicates its appreciable complexation with the polymer matrix or its complete dissolution in the host polymers. **Sharma et al.** [50], in their PEO-PMMA-PEG polymer blend electrolytes, discussed the similar observations.

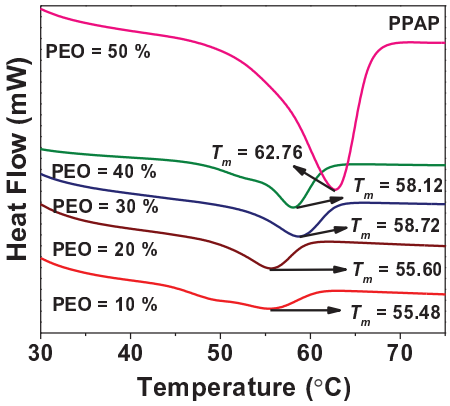

Fig. 4.13 DSC scans of blend specimens of PPAP series for varying PEO amounts

Table 4.7 Variation in melting temperatures (T_m) and degree of crystallinity (X_c) of blend specimens of PPAP series for varying PEO concentrations

PEO *(%)*	Melting Temperature *(T_m) (°C)*	Degree of Crystallinity *(%X_c)*
10	55.48	74.59
20	55.60	70.05
30	58.72	68.02
40	58.12	66.67
50	62.76	62.84

DSC scans of the blend specimens of PPAP series with different PEO concentrations as shown in Fig. 4.13 show presence of a single endothermic peak in the range of 55 °C to 63 °C which corresponds to the melting of PEO in the respective blend specimen. With the variation in PEO content, this melting peak shifts randomly which indicates the inter-molecular interaction, compatibility and hence, miscibility amongst the pure PVA and PEO polymers [51-53]. The values of melting temperature (T_m) corresponding to these melting peaks as listed in Table 4.7 are found to be quite near to the 'T_m' values of pure PEO polymer. Further, degree of crystallinity 'X_c' for each blend specimen as calculated and listed in Table 4.7 is found to reduce systematically with the increasing amount of PEO in the blends which suggests the consistent lowering of crystallinity with the simultaneous enhancement in the amorphous phases in the blends. **Senthil et al.** [54] too observed similar results for their guanine incorporated polymer blend electrolyte.

FT-IR spectra of the blends at each PEO concentration are shown in Fig. 4.14 and the corresponding band positions and their assignments are listed in Table 4.8. These FT-IR spectra show the presence of the features of both PVA as well as PEO polymers. A band appearing nearly at 3400 cm^{-1} to 3200 cm^{-1} in the FT-IR spectrum of the blend with 10 % of

PEO, gradually broadens along with the simultaneous reduction in its intensity and finally covers a broader range of wavenumber from 3500 cm^{-1} to 3100 cm^{-1} in case of the specimen with 50 % of PEO.

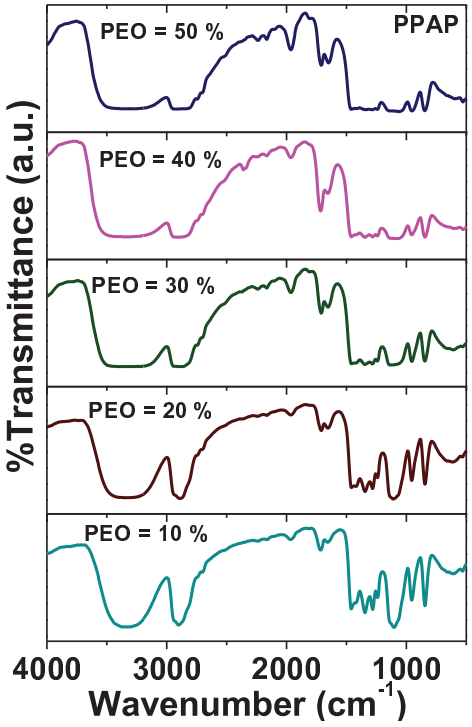

Fig. 4.14 FT-IR spectra of blend specimens of PPAP series for varying PEO contents

Table 4.8 Vibrational modes & wavenumbers exhibited by the blend specimens of PPAP series for varying PEO contents

Wavenumber (cm^{-1})	Assignment
3538-3115	Intermolecular OH Stretching (hydroxyl) band of PVA: characteristic feature of alcohols
2939	C-H Stretching of CH_2 of PVA
2241	C–H Stretching of PEO/ C=O Combination of PEO
2165	Asymmetric C–H Stretching of PEO/ C–H Deformation Combination of PEO
1962	Asymmetric Stretching Band of PEO
1724	C=O Stretching of PVA
1647	C=C Stretching of PVA
1466	CH_2 Scissoring of PEO
1348	CH_2 Wagging of PEO
1280	Asymmetric CH_2 Twisting of PEO
1235	C-C Stretching of PVA/ C-H Wagging of PVA
1104	C-O-C Stretching of PEO
950	CH_2 Symmetric Rocking of PEO/ C–O–C Stretching of PEO
846	C-C Stretching of PVA
640	OH Twisting of PVA

The range of this band indicates that it corresponds to the intermolecular –OH stretching (hydroxyl) of PVA. In addition to this feature, as the amount of PEO increases in the blends, the intensity of the peak appearing at nearly 2939 cm^{-1} corresponding to C-H stretching of CH_2 of PVA gradually reduces making it substantially broader. Also, a small kink at nearly 1235 cm^{-1} with respect to the C-C stretching of PVA/C-H wagging of PVA and a peak at 846 cm^{-1} referring to C-C stretching of PVA gradually diminish with the addition of PEO in the blends. However, the intensities of small peaks at about 1724 cm^{-1} and 1647 cm^{-1} corresponding to C=O stretching of PVA and C=C stretching of PVA respectively, increases slightly with the incorporation of PEO in the blends.

In addition to these features, the FT-IR spectra also shows the presence of several intense peaks and kinks in the wavenumber range of 1500 cm^{-1} to 500 cm^{-1}. The assignments of peak positions are listed in Table 4.8. As the amount of PEO increases in the blends, the intensity of these peaks and kinks decrease gradually. A small peak appearing at 1962 cm^{-1} corresponding to asymmetric stretching band of PEO becomes gradually intense with respect to PEO concentration. Reduction in intensity of peaks and broadening of the bands indicates the increment in the amorphicity of the blend matrix. The intensity of almost all the features observed in the FT-IR spectra of the blend specimens is considerably lower than those seen for the pure polymers, indicating good complexation of both the polymers and increase of amorphous nature. **Aram et al.** [55] pointed out the increase in amorphicity in PEO/PMMA gel electrolyte system, due to reduction in IR intensity.

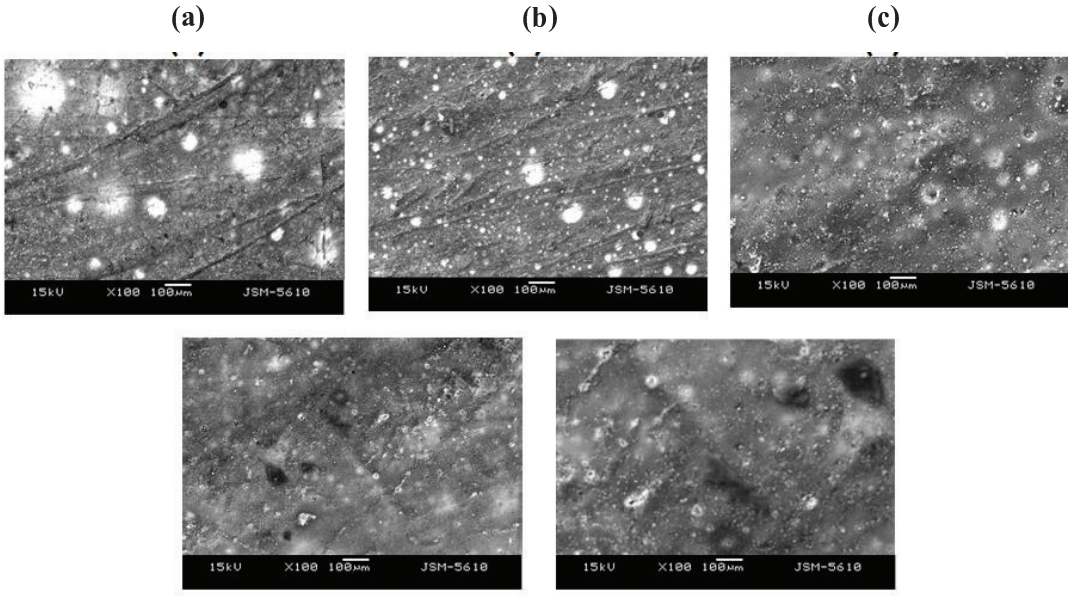

Fig. 4.15 SEM images of blend specimens of PPAP series for (a) PEO = 10 %, (b) PEO = 20 %, (c) PEO = 30 %, (d) PEO = 40 % and (e) PEO = 50 %

The SEM images of the blends of PPAP series for different PEO contents are depicted in Fig. 4.15 (a) to (e), respectively. For the specimen with 10 % of PEO, the image shows the presence of big white spots spread almost uniformly in the grey coloured surface of the blend.

But with the increasing amount of PEO in the blend, the size as well as the number of these white spots reduces significantly. Moreover, with the rising content of PEO in the specimens, black spots resembling the pores are also observed. Such characteristic porous microstructure is also observed in the SEM image of pure PEO and PEO based electrolytes prepared by the solvent casting method by **Pradeepa et al.** [13] and the **Das group** [46]. These pores aid in entrapping or storing a large amount of liquid solution (salt and plasticizer mixtures) [13]. These pores become large and prominent with further addition of PEO beyond 30 % in blend.

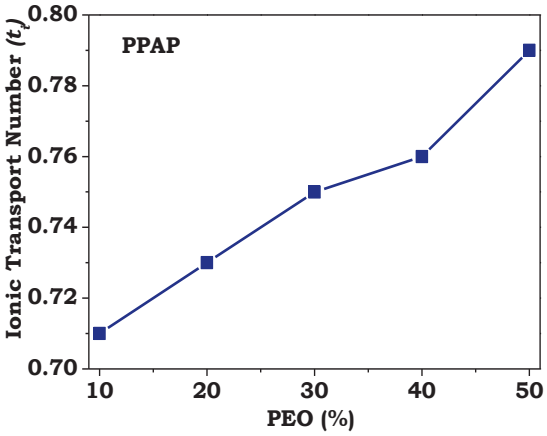

Fig. 4.16 Variation in ionic transport number (t_i) of blend specimens of PPAP series for different PEO concentrations

Variation in the ionic transport number (t_i) with respect to the PEO concentrations as shown in Fig. 4.16 indicates the systematic enhancement in the 't_i' values with increasing PEO content in the blends. Basically, the ether oxygens present in the chains of PEO polymer not only aid in the dissociation of the salt incorporated in the polymer but their sufficient donor power facilitates to form the coordinate bonds with the cations of the salt. These ether oxygens allow multiple intra-polymer ion bonding with low barriers for rotations of atoms in main chain further, enhancing the flexibility as well as the segmental mobility and leading to the gradual enhancement in the ionic transport number (t_i) with respect to PEO concentration.

4.4 [$PVA_{(50)}$: $PEO_{(50)}$] – 5 wt% $AgNO_3$ – 10 wt% PEG – x wt% Al_2O_3 (PPAPA) Series

As the specimen with 50 % of PEO of PPAP series depicts the optimum amorphicity as well as ionic transport number of the rest of the blends, it chosen as the base electrolyte for the preparation of the next nano-composite PPAPA series given as '[$PVA_{(50)}$: $PEO_{(50)}$] – 5 wt% $AgNO_3$ – 10 wt% PEG – x wt% Al_2O_3' wherein, the Al_2O_3 concentration is varied from 2 wt% to 10 wt%. Various characteristic properties of these blends are further investigated in detail and discussed thoroughly.

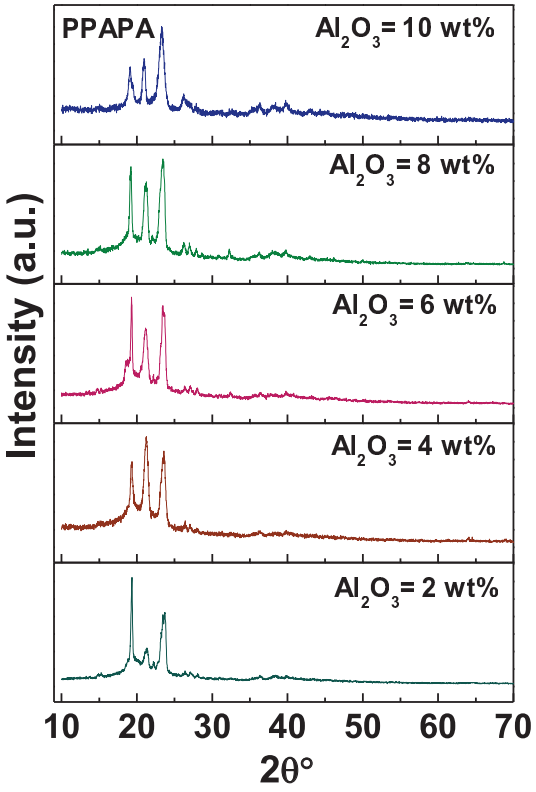

Fig. 4.17 XRD scans of blend specimens of PPAPA series for varying Al_2O_3 amounts

XRD patterns of the blends of the PPAPA series as shown in Fig. 4.17 for varying amounts of Al_2O_3 nano-filler depicts the presence of the three major peaks at ~ 19°, ~ 21° and ~ 23° corresponding to pure PEO. The intensity of the peaks at ~ 19° and ~ 21° vary randomly with Al_2O_3 concentration but the peak at about ~ 23° becomes gradually intense but

broadens slightly with the increasing content of Al_2O_3 in the blends. The observations suggest that the incorporation of Al_2O_3 nano-filler in the blends makes the polymeric molecular chain amorphous and leads to some structural reorganization such as disruption of the chain packing, weakening of the intermolecular interactions and increase in the volume, thus, reducing the crystallinity of the blend matrix [21,56,57].

DSC thermograms of the blend specimens of PPAPA series with different amounts of Al_2O_3 nano-filler are shown in Fig. 4.18. For each concentration of Al_2O_3, the respective DSC scans show the presence of a sharp endothermic peak corresponding to the melting of PEO polymer. The melting temperatures (T_m) vary in a random fashion with respect to Al_2O_3 amounts [51-53]. These melting temperatures of blend specimens of PPAPA series lie in range of 59 °C to 64 °C, as seen from Table 4.9. Further, as the amount of Al_2O_3 nano-filler is increased in the blends, a gentle observation of the DSC scans shows an interesting feature of the gradual formation of a small endothermic peak (marked with an arrow) in the temperature range of 50 °C to 55 °C with addition of Al_2O_3 upto 6 wt%. But beyond 6wt% of Al_2O_3, this endothermic peak gradually suppresses and completely loses its existence in case of the blend with 10 wt% of Al_2O_3. Such a double peak feature as observed in the DSC scans of the present nano-composite blends are also observed by **Sumathipala et al.** [58] and **Sultana et al.** [59] in their PEO-LiBOB-CP-SZ and TlI-Al_2O_3 composite systems, respectively. Such an endothermic peak within the temperature range of 50 °C to 55 °C in the present case is expected to occur due to uneven dispersion of Al_2O_3 nano-filler in PVA-PEO blend phase.

The variation in the degree of crystallinity (X_c) with increasing Al_2O_3 concentrations is given in Table 4.9 wherein, the 'X_c' values reduce gradually with the initial rise in Al_2O_3 concentration upto 6 wt%. This may be related to uneven dispersion of nano-particles between polymeric chains which in turn may induce the structure modification of polymer

chains. Such a phenomenon may lead to the systematic formation of favourable conductive pathways for the mobility of ions on the surface of nano-filler. But with the further increase of Al_2O_3 amount > 6 wt%, 'X_c' values increase slightly.

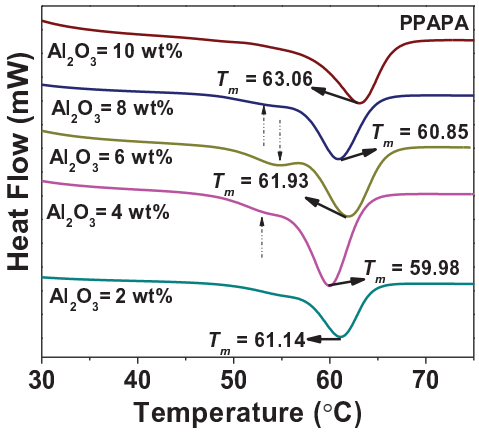

Fig. 4.18 DSC scans of blend specimens of PPAPA series for varying Al_2O_3 amounts

Table 4.9 Variation in melting temperatures (T_m) and degree of crystallinity (X_c) of blend specimens of PPAPA series for varying Al_2O_3 concentrations

Al_2O_3 *(wt%)*	Melting Temperature *(T_m)(°C)*	Degree of Crystallinity *(%X_c)*
2	61.14	58.56
4	59.98	51.55
6	61.93	42.07
8	60.85	62.54
10	63.06	73.91

Similar discussion is carried out by **Chandra et al.** [60] in sodium ion conducting nano composite polymer electrolytes and by **Zhai et al.** [61] in nano-TiO_2 based PVdF-HFP nanocomposite polymer electrolyte. **Ketabi et al.** [62] in their discussion for SiO_2 and TiO_2 nano-filler in poly(ethylene oxide)–$EMIHSO_4$ electrolytes, described the disruption of reordering of polymer chains.

The FT-IR spectra of the blend specimens at various Al_2O_3 concentrations are shown in Fig. 4.19. Most of the bands, peaks and kinks as assigned in Table 4.10 are commonly observed in the respective FT-IR spectrum of each nano-composite blend specimen of PPAPA series. As observed from the figure, no considerable variation in the positions of the features is observed with the changes in the amounts of Al_2O_3 nano-filler. However, the intensities of almost all the peaks and kinks are found to reduce slightly with the increasing amount of Al_2O_3 nano-filler but upto 6 wt% only. Such an observation indicates that the amorphicity of the blend matrix augments gradually with respect to Al_2O_3 concentration. Similar variation is observed by **Sharma et al.** [57] in their Al_2O_3 based PEO-PMMA-PEG-

$AgNO_3$ system. But on the other hand, beyond the addition of 6 wt% of Al_2O_3 in the present case, these peaks and kinks get substantially intense.

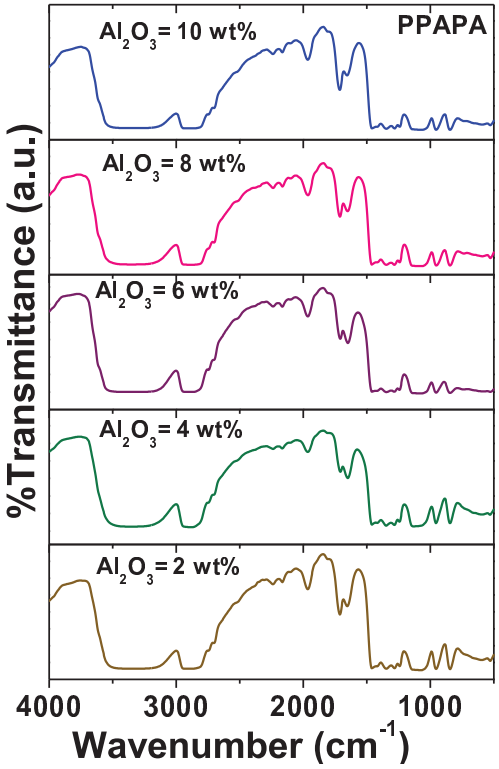

Fig. 4.19 FT-IR spectra of blend specimens of PPAPA series for varying Al_2O_3 contents

Table 4.10 Vibrational modes & wavenumbers exhibited by the blend specimens of PPAPA series for varying Al_2O_3 contents

Wavenumber (cm^{-1})	Assignment
3550-3100	Intermolecular OH Stretching (hydroxyl) band of PVA: characteristic feature of alcohols
2935-2800	C–H Stretching of PEO
2241	C–H Stretching of PEO/ C=O Combination of PEO
2165	Asymmetric C–H Stretching of PEO/ C–H Deformation Combination of PEO
1962	Asymmetric Stretching Band of PEO
1724	C=O Stretching of PVA
1647	C=C Stretching of PVA
1466	CH_2 Scissoring of PEO
1348	CH_2 Wagging of PEO
1280	Asymmetric CH_2 Twisting of PEO
1235	C-C Stretching of PVA/ C-H Wagging of PVA
1104	C-O-C Stretching of PEO
950	CH_2 Symmetric Rocking of PEO/ C–O–C Stretching of PEO
846	C-C Stretching of PVA
640	OH Twisting of PVA

SEM images of the blend specimens for varying amounts of Al_2O_3 nano-filler are depicted in Figs. 4.20 (a) to (e), respectively. At 2 wt% of nano-filler, the surface of the blend shows small black pores along with the white patches. The white patchy regions refer to the crystalline phases of the blend matrices whereas; the small pores present on the blend surfaces correspond to the amorphous phases present therein. With the increasing amount of Al_2O_3 upto 6 wt%, the pores begin to gain prominence. But beyond this concentration of nano-filler, the white patches on the blends' surfaces increase and the films seem to get rougher. This suggests that with the increasing content of Al_2O_3 upto 6 wt%, the degree of crystallinity gradually drops down but with the further rise in the amount of Al_2O_3, the reverse phenomenon occurs.

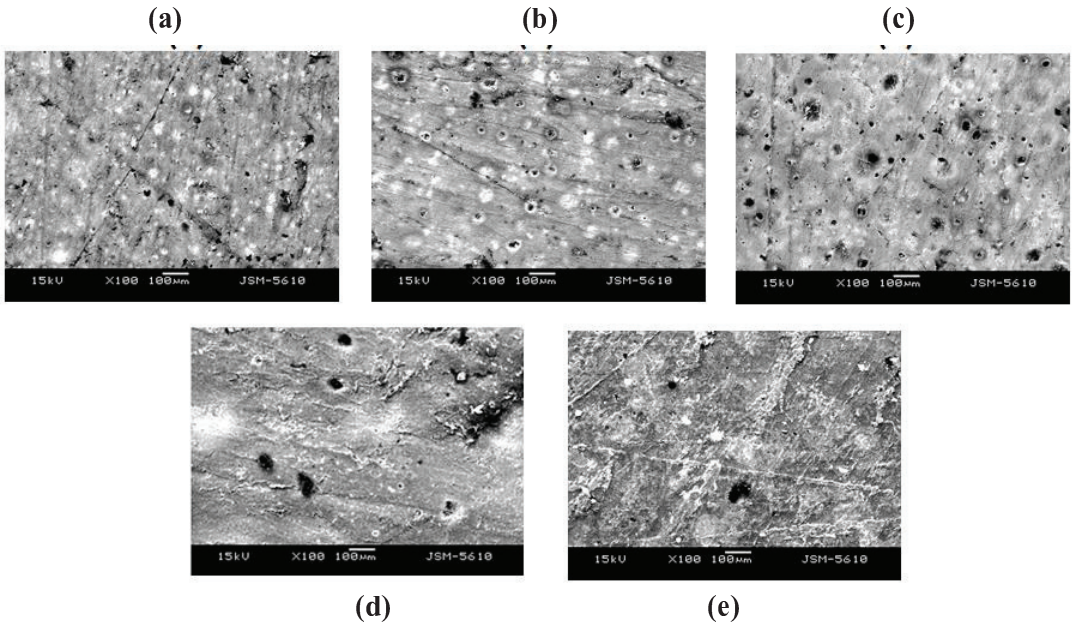

Fig. 4.20 SEM images of blend specimens of PPAPA series for (a) Al_2O_3 = 2 wt%, (b) Al_2O_3 = 4 wt%, (c) Al_2O_3 = 6 wt%, (d) Al_2O_3 = 8 wt% and (e) Al_2O_3 = 10 wt%

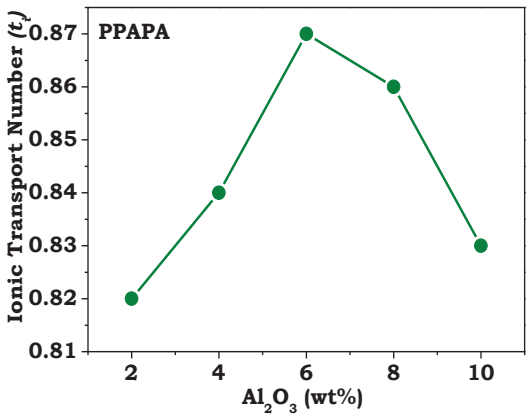

Fig. 4.21 Variation in ionic transport number (t_i) of blend specimens of PPAPA series for different Al_2O_3 concentrations

Fig. 4.21 shows the variation in ionic transport number 't_i' of blends of PPAPA series with respect to Al_2O_3 amounts. When the amount of nano-filler in the blend matrix is less, the filler particles are sufficiently separated from each other which in turn create the free volume in the blend matrix and facilitate the conducting pathways for the movement of Ag^+. Owing to these processes, the ionic transport number 't_i' increases significantly with the addition of Al_2O_3 in blends. But such a phenomenon takes place only upto 6 wt% of Al_2O_3 in blends as beyond this concentration of nano-filler, the filler particles are likely to get so close to each

other that they form neutral aggregates. These neutral aggregates not only increase the crystalline phases of the blend matrix thus, reducing its free volume and amorphicity but also block the conducting pathways through which the mobile Ag^+ can conduct. Owing to this reason, the values of ionic transport number (t_i) drop significantly with the addition of Al_2O_3 beyond 6 wt% in blends.

4.5 [$PVA_{(50)}$: $PEO_{(50)}$] – 5 wt% $LiCF_3SO_3$ – x wt% EC (PPLE) Series

A new series with EC plasticizer and $LiCF_3SO_3$ salt is prepared and given as '[$PVA_{(50)}$: $PEO_{(50)}$] – 5 wt% $LiCF_3SO_3$ – x wt% EC' wherein; the amount of EC plasticizer is varied from 2 wt% to 10 wt%. X-ray spectra of the specimens of this series are depicted in Fig. 4.22.

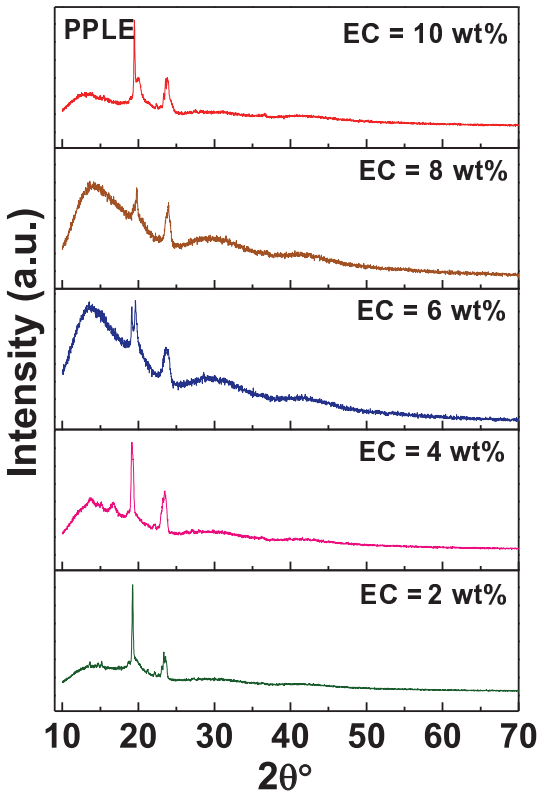

Fig. 4.22 XRD scans of blend specimens of PPLE series for varying EC amounts

A broad peak positioning at about ~ 19° in the XRD spectrum of pure PVA polymer also appears in the XRD scan of the EC plasticized specimen with EC = 2 wt% as a small broad hump, but at a shifted position of 2θ ~ 14°. As the amount of EC in blends increases upto 6

wt%, the hump remains nearly at the same position but broadens slightly. But with the further increase in the EC concentration beyond 6 wt%, this broad hump suppresses gradually. Additionally, a sharp intense peak appearing at ~ 19° resembling to the peak of pure PEO, which loses its intensity, getting systematically broader with addition of EC upto 6 wt%, starts gaining its sharpness and intense character at EC > 6 wt%. Further, a small peak is also observed at ~ 23° in the XRD spectra of all the blend specimens. However, the intensity of this peak fluctuates with respect to EC concentrations in the blends. In addition to these features, two wide and broad humps at ~ 29° and ~ 40° gradually appear as EC is added in the blends upto 6 wt% where, the hump at ~ 40° is clearly said to be associated with pure PVA polymer. Such a new peak appearing in the XRD spectrum of the respective blend specimen is expected to correspond to the PVA-PEO blend phase. However, the one at ~ 29° is neither related to PVA nor to PEO polymers. Moreover, EC possesses high dielectric constant value (89.8) which aids in dissociating both ion pairs and ion aggregates thus, leading to higher number density of free ions and facilitating the coupling synergy between ionic motion and polymer segmental motion [44,63-66]. But beyond 6 wt% of EC, both these broad humps subsequently diminish and finally lose their individuality at EC = 10 wt% which suggests that at higher concentrations of EC above 6 wt%, the amorphicity of the specimens drop down significantly thus, enhancing the crystalline phases in the blend matrix.

DSC thermograms of the blends at different EC plasticizer concentrations in the range of 2 wt% to 10 wt% are shown in Fig. 4.23 which show presence of a single endothermic peak corresponding to the melting of PEO polymer in respective blend specimen. Upto 6 wt% of EC, this peak shifts towards the higher temperature side but at the higher EC concentration > 6 wt%, the peak systematically shifts towards lower temperature side. Also, the values of melting temperatures (T_m) of the blend specimens lying in the range of 57 °C to 62 °C are listed in Table 4.11. **Saroj et al.** [67] mentioned about the occurrence of similar phenomenon

taking place in their ionic liquid based electrolyte system. Further, in the present case, the values of degree of crystallinity (X_c) is calculated for different concentrations of EC plasticizer in blends and given in Table 4.11.

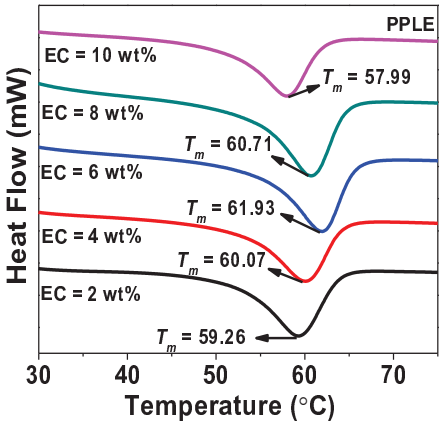

Fig. 4.23 DSC scans of blend specimens of PPLE series for varying EC amounts

Table 4.11 Variation in melting temperatures (T_m) and degree of crystallinity (X_c) of blend specimens of PPLE series for varying EC concentrations

EC *(wt%)*	Melting Temperature *(T_m)(°C)*	Degree of Crystallinity *(%X_c)*
2	59.26	89.84
4	60.07	74.50
6	61.93	72.33
8	60.71	79.51
10	57.99	87.92

The decrease in the 'X_c' values with the addition of EC upto 6 wt% is because of the gradual reduction in the internal viscosity of the blend films. This in turn enhances flexibility of the polymeric chains. **Johan et al.** [38] also substantiated similar results for their PEO–$LiCF_3SO_3$–EC system. In the present case, at EC > 6 wt% 'X_c' values start enhancing which suggests that the crystallinity of the blend matrices begins to increase beyond certain amount of plasticizer therein.

FT-IR spectra of the blends of PPLE series with different EC contents are depicted in Fig. 4.24 and the assignments of the bands, peaks and kinks appearing in the respective spectrum are mentioned in Table 4.12. As observed from the FT-IR spectra, a broad band appearing in range of 3500 cm^{-1} to 3200 cm^{-1}, 2950 cm^{-1} to 2850 cm^{-1} and the features arising in the range of 1500 cm^{-1} to 500 cm^{-1} gradually reduce their intensity with enhancement of EC plasticizer in the blends upto 6 wt%. However, beyond 6 wt% of EC in the blends, the as mentioned peaks and the features regain their intense nature back. **Woo et al.** [64] in their EC based solid polymer electrolyte system also reported the similar results. The observations

appearing in the FT-IR spectra of the present study suggest that initially, with the addition of EC upto 6 wt%, the amorphicity of blend matrix enhances but beyond this concentration, degree of crystallinity begins to increase.

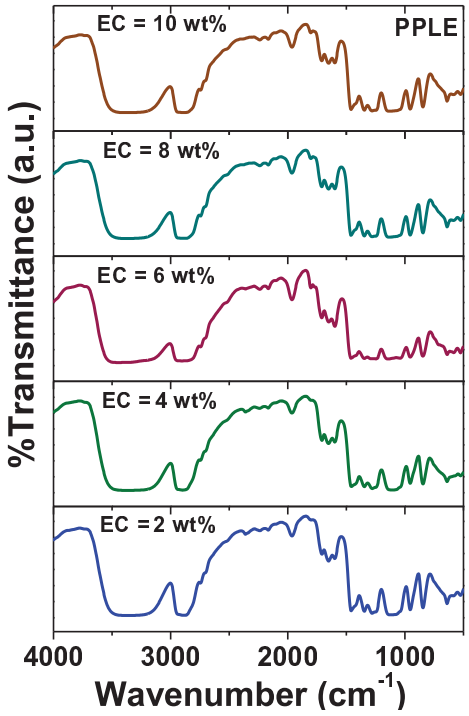

Fig. 4.24 FT-IR spectra of blend specimens of PPLE series for varying EC contents

Table 4.12 Vibrational modes & wavenumbers exhibited by the blend specimens of PPLE series for varying EC contents

Wavenumber (cm^{-1})	Assignment
3550-3100	Intermolecular OH Stretching (hydroxyl) band of PVA: characteristic feature of alcohols
2935-2800	C–H stretching of PEO
2376	C=C Stretching of PEO
2241	C–H Stretching of PEO/ C=O Combination of PEO
2165	Asymmetric C–H Stretch of PEO/ C–H Deformation Combination of PEO
1962	Asymmetric Stretching Band of PEO
1724	C=O Stretching of PVA
1647	C=C Stretching of PVA/
1596	C=C Stretching of PEO
1466	CH_2 Scissoring of PEO
1348	CH_2 Wagging of PEO
1280	Asymmetric CH_2 Twisting of PEO
1104	C-O-C Stretching of PEO
950	CH_2 Symmetric Rocking of PEO/ C–O–C Stretching of PEO
842	CH_2 Twisting of PEO/ CH_2 Wagging of PEO
640	OH Twisting of PVA
528	C-O-C Bending of PEO

Morphological studies comprise of the detailed study of the SEM images of the blend specimens with different EC concentrations, as shown in Fig. 4.25 (a) to (e). For the blend with 2 wt% of EC, the SEM image shows quite a rough surface. But with gradual addition of EC upto 6 wt%, the surface gradually gets smoother. Such a phenomenon indicates the systematic increment in the amorphous phase in the blend matrix with respect to the amount of EC plasticizer in blends [7,68,69]. But at EC > 6 wt%, the surface of the blend systematically regains its roughness which indicates that when the plasticizer is added in blends beyond a certain amount, it degrades the amorphous phase of the blend matrix.

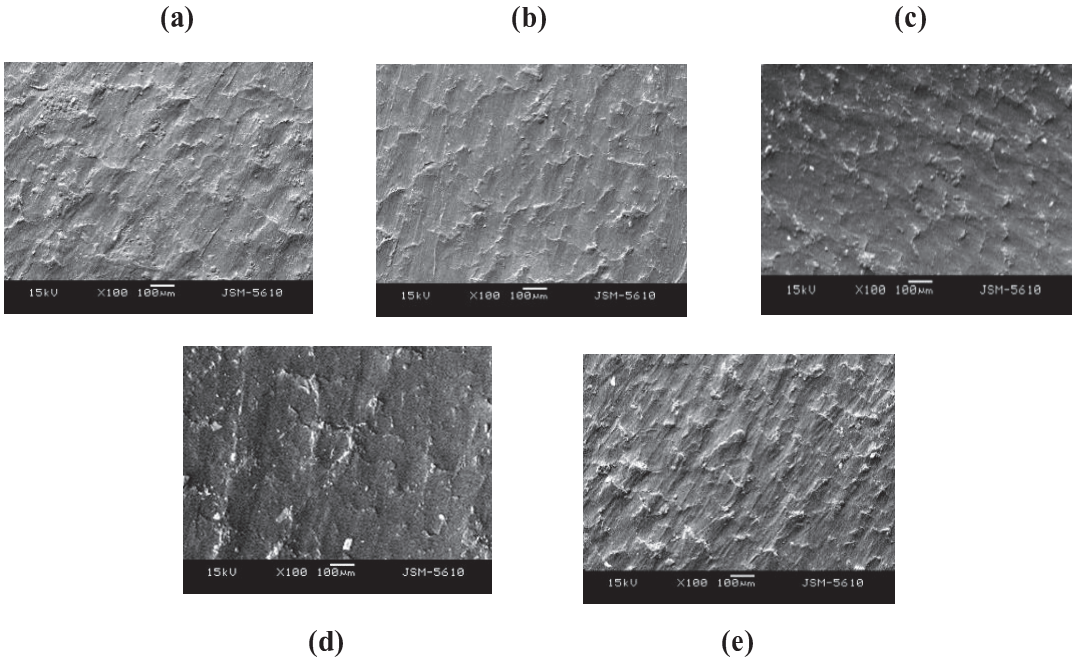

Fig. 4.25 SEM images of blend specimens of PPLE series for (a) EC = 2 wt%, (b) EC = 4 wt%, (c) EC = 6 wt%, (d) EC = 8 wt% and (e) EC = 10 wt%

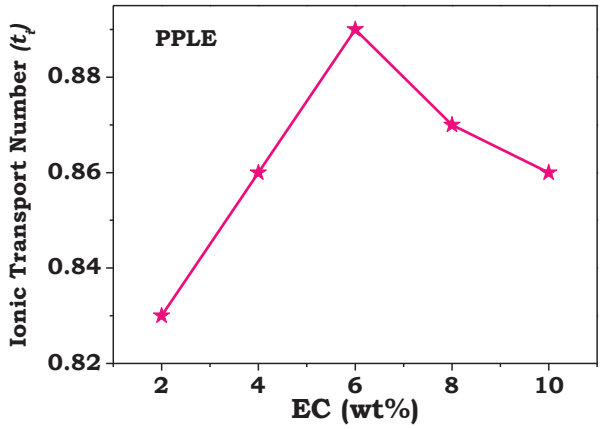

Fig. 4.26 Variation in ionic transport number (t_i) of blend specimens of PPLE series for different EC concentrations

The increment in the values of ionic transport number 't_i' increases with EC content in blends upto 6 wt% and thereafter 't_i' decreases as seen from Fig. 4.26. Interestingly, with increasing content of plasticizer in blends, the process of salt dissociation gets significantly active hence, producing more and more free charge carriers which in turn participate in the conduction process. But at EC > 6 wt% the number of free Li^+ and $CF_3SO_3^-$ become so high

that instead of yielding conductivity, they come closer to each other and start coordinating to form neutral aggregates. These neutral aggregates in turn block the conducting pathways and increase the degree of crystallinity of the blend matrix thus, reducing its amorphicity. All these factors in turn restrict the mobility of free cations and anions participating in process of conduction and drop down the values of ionic transport number 't_i' at EC > 6 wt% in blends.

4.6 [$PVA_{(50)}$: $PEO_{(50)}$] – 6 wt% EC – x wt% $LiCF_3SO_3$ (PPEL) Series

As observed for PPLE series, the blend specimen with 6 wt% of EC plasticizer showed the optimum level of amorphicity and ionic transport number out of the rest of the blends. Hence, considering this amount of EC as constant, blends of the next series i.e. PPEL series given as '[$PVA_{(50)}$: $PEO_{(50)}$] – 6 wt% EC – x wt% $LiCF_3SO_3$' are prepared wherein concentrations of $LiCF_3SO_3$ salt is varied in the range of 3 wt% to 11 wt%. The characterization studies of all these blends are carried out and analysed thoroughly.

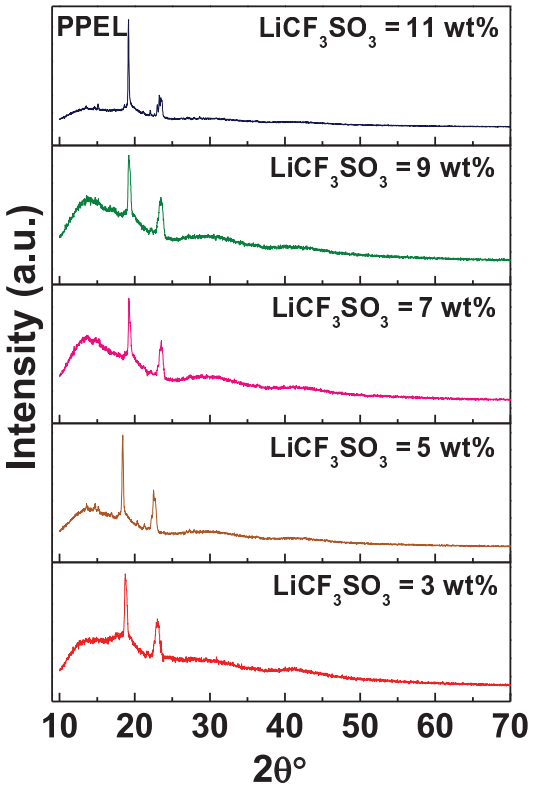

Fig. 4.27 XRD scans of blend specimens of PPEL series for varying $LiCF_3SO_3$ amounts

The XRD scans of the blend specimens of the PPEL series as depicted in the Fig. 4.27 show similar features as shown by the specimens PPLE series. The broad hump occurring at ~ 19° in the XRD spectrum of PVA polymer gets shifted to ~ 14° in XRD scan of the specimen with 3 wt% of $LiCF_3SO_3$. However, with further addition of salt upto 9 wt%, this hump becomes more prominent and broader and beyond this salt concentration, the hump gets slightly suppressed. Similarly, two small broad humps at ~ 29° and ~ 40° gradually appear and become prominent with the addition of salt upto 9 wt%. But at 11 wt% of the salt, these humps completely disappear. Intensity of the peak at ~ 23° remains almost unchanged with respect to salt concentration but of the sharp peak at ~ 19° decreases slightly making it broader, with substantial addition of $LiCF_3SO_3$ salt upto 9 wt%. Beyond this salt concentration, the peak gets significantly sharp and intense. Similar features were discussed by **Pradeepa et al.** [13], **Kesavan et al.** [69], **Kumar et al.** [70], **Muthuvinayagam et al.** [71], **Pandi et al.** [72] and **Ni'mah et al.** [73]. An enhancement in the amorphous phase with the increment of salt content upto 9 wt% in the blends causes a reduction in the energy barrier which in turn favours easy segmental motion of the polymer electrolyte chains. Further incorporation of salt beyond 9 wt%, makes the peak(s) highly intense and sharp similar to that observed by **Kumar et al.** [70], indicating the reformation of crystalline phases in the blend matrix.

DSC thermograms of the blends specimens with different amounts of $LiCF_3SO_3$ salt are shown in Fig. 4.28 wherein, each DSC scan depicts the presence of a single endothermic peak corresponding the melting of PEO in the respective blend specimen. These melting peaks shift systematically towards lower temperature side with the addition of $LiCF_3SO_3$ salt in blends upto 9 wt%. But at $LiCF_3SO_3$ = 11 wt%, the peak shifts towards higher temperature side. Values of the melting temperatures (T_m), as depicted in Table 4.13 lie in range of 59 °C to 64 °C. The gradual reduction in melting temperatures is associated with the difference

between the forces of attraction amongst the polymer chains in the regularly packed crystalline state and the disordered liquid phase. It means that the strength of intermolecular forces gets reduced with the addition of salt in blends.

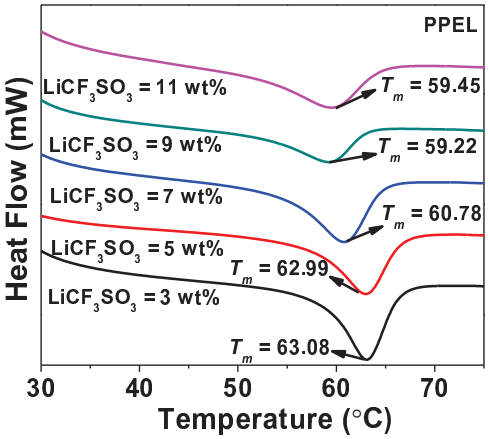

Fig. 4.28 DSC scans of blend specimens of PPEL series for varying $LiCF_3SO_3$ amounts

Table 4.13 Variation in melting temperatures (T_m) and degree of crystallinity (X_c) of blend specimens of PPEL series for varying $LiCF_3SO_3$ concentrations

$LiCF_3SO_3$ *(wt%)*	Melting Temperature *(T_m)(°C)*	Degree of Crystallinity *(%X_c)*
3	63.08	47.17
5	62.99	43.50
7	60.78	39.79
9	59.22	32.24
11	59.45	34.30

In crystalline state, entropy is small, chains are stiff and melting temperature 'T_m' is higher. It means that, with the initial addition of salt, stiffness of polymer chains and steric effect reduce the 'T_m' values due to the presence of salt dissociation. But at 11 wt% of salt, flexibility of the polymeric chains decreases due to the presence of non-dissociated bulky $LiCF_3SO_3$ salt between the chains of polymer.

The FT-IR spectra of the blends at different $LiCF_3SO_3$ salt concentration are as shown in Fig. 4.29. The assignments of the bands, peaks and kinks observed in these spectra are listed in Table 4.14. The figure shows two broad bands appearing in the range of 3550 cm^{-1} to 3100 cm^{-1} and 2935 cm^{-1} to 2800 cm^{-1} in case of the blend with 3 wt% of salt. With further addition of salt upto 9 wt%, these bands gradually broaden. These are typical PVA and PEO features as shown in Figs. 4.10 and 4.11, respectively. As seen from Fig. 4.29, most of the features existing between 1500 cm^{-1} to 800 cm^{-1} are also observed in PEO's FT-IR spectrum as shown in Fig. 4.11. In addition to these features corresponding to PEO polymer, some of the feature resembling to PVA polymer as seen from Fig. 4.10, are also observed in FT-IR

spectrum corresponding to each respective blend specimen of PPEL series. However, many features are suppressed and very low intensity peaks are seen with addition of salt in blends which confirms the complexation of salt and blending of polymers. However, beyond 9 wt% of salt concentration the bands at 3550 cm^{-1} to 3100 cm^{-1} and 2935 cm^{-1} to 2800 cm^{-1} and the peaks in the range of 1500 cm^{-1} to 800 cm^{-1} become slightly intense.

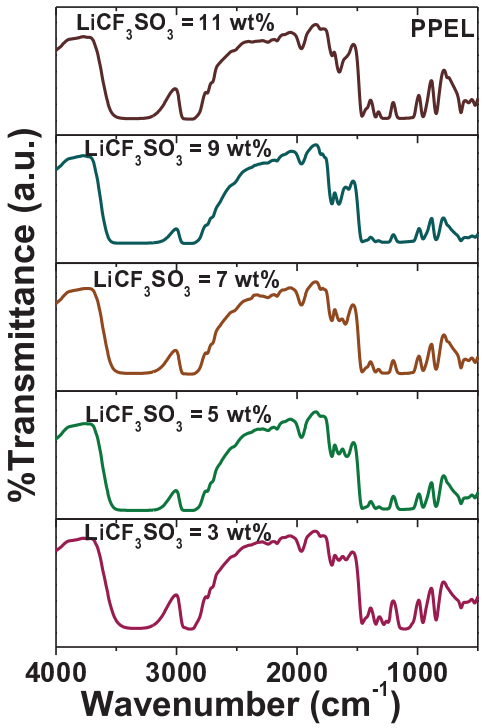

Fig. 4.29 FT-IR spectra of blend specimens of PPEL series for varying $LiCF_3SO_3$ contents

Table 4.14 Vibrational modes & wavenumbers exhibited by the blend specimens of PPEL series for varying $LiCF_3SO_3$ contents

Wavenumber (cm^{-1})	Assignment
3550-3100	Intermolecular OH Stretching (hydroxyl) band of PVA: characteristic feature of alcohols
2935-2800	C–H stretching of PEO
2241	C–H Stretching of PEO/ C=O Combination of PEO
2165	Asymmetric C–H Stretching of PEO/ C–H Deformation Combination of PEO
1962	Asymmetric Stretching Band of PEO
1724	C=O Stretching of PVA
1647	C=C Stretching of PVA
1596	C=C Stretching of PEO
1466	CH_2 Scissoring of PEO
1348	CH_2 Wagging of PEO
1280	Asymmetric CH_2 Twisting of PEO
1235	C-C Stretching of PVA/ C-H Wagging of PVA
1104	C-O-C Stretching of PEO
950	CH_2 Symmetric Rocking of PEO/ C–O–C Stretching of PEO
842	CH_2 Twisting of PEO/ CH_2 Wagging of PEO
640	OH Twisting of PVA
528	C-O-C Bending of PEO

Such variations in the FT-IR spectra of the blends with the addition of $LiCF_3SO_3$ salt may be due to the interaction between the chains of polymers of the blends and co-ordination interaction between the salt and polymeric groups. However, no features corresponding to $LiCF_3SO_3$ salt are observed in any of the FT-IR spectra which may be due to the disruption of initial order of polymer blend with the addition of lithium salt and its good complexation with polymer matrix [7].

The SEM images of the blends at different $LiCF_3SO_3$ salt concentrations are shown in Fig. 4.30 (a) to (e). As observed from the images, as the amount of $LiCF_3SO_3$ salt in the blends increases, the surfaces of the respective blends changes gradually. Smoothening of the blend surfaces with the rise in salt content upto 9 wt% is an indicative of systematic increase in the amorphous phase in the blend polymer electrolyte complex which is mainly due to the gradual dissolution of salt in the polymer matrix [7,60,71]. However, at 11 wt% of salt, the surface gets slightly rough and the morphology changes. Such a rough morphology may be because of agglomerated salt particles which could not be dissociated in blend matrix [63,74].

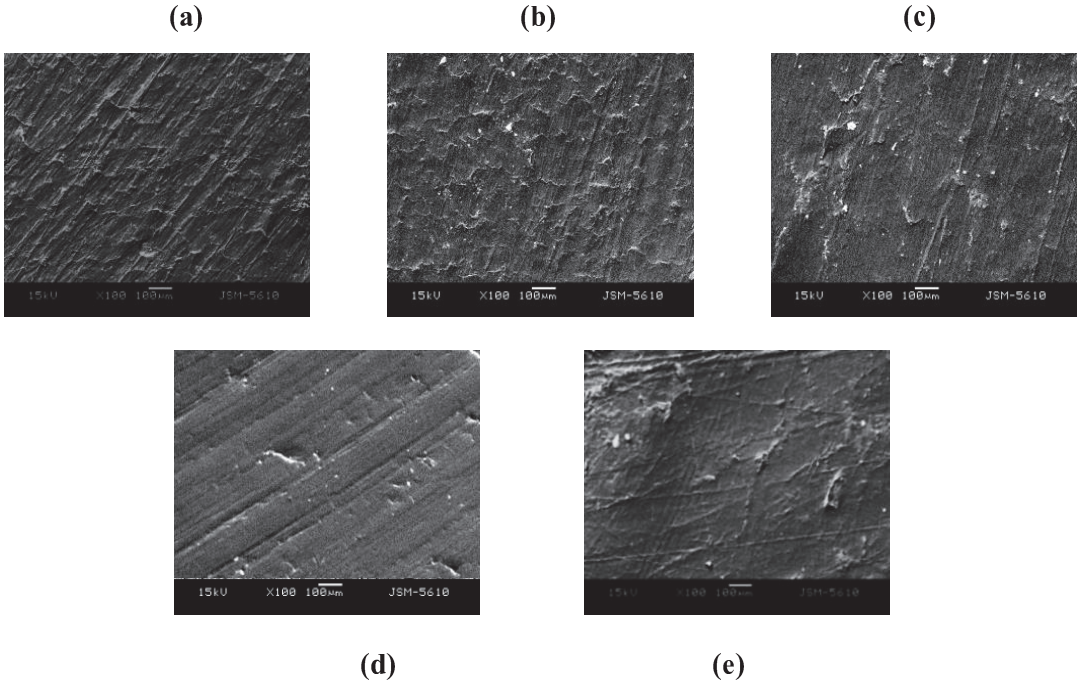

Fig. 4.30 SEM images of blend specimens of PPEL series for (a) $LiCF_3SO_3$ = 3 wt%, (b) $LiCF_3SO_3$ = 5 wt%, (c) $LiCF_3SO_3$ = 7 wt%, (d) $LiCF_3SO_3$ = 9 wt% and (e) $LiCF_3SO_3$ = 11 wt%

The plot of ionic transport number (t_i) with varying amount of $LiCF_3SO_3$ salt has been depicted in Fig. 4.31 which shows the rise in the value of ionic transport number 't_i' with the doping of salt upto 9 wt% beyond which this value drops down. Here, with the initial addition of salt, due to salt dissociation, the number of free Li^+ and $CF_3SO_3^-$ in the blend matrix increase leading to gradual improvement in 't_i' values.

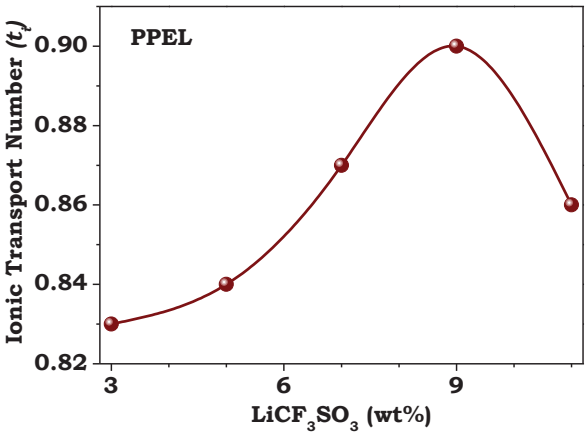

Fig. 4.31 Variation in ionic transport number (t_i) of blend specimens of PPEL series for different $LiCF_3SO_3$ concentrations

However, at higher content of salt of 11 wt%, these free charge carriers start reassociating with each other and form neutral aggregates. This phenomenon in turn lowers the number of free charge carriers participating in the conduction process hence, dropping the 't_i' value. Such a variation in the ionic transport number 't_i' values with respect to $LiCF_3SO_3$ salt concentrations is supported by other studies viz. XRD, DSC, FT-IR and SEM also.

4.7 [$PVA_{(50)}$: $PEO_{(50)}$] – 6 wt% EC– 9 wt% $LiCF_3SO_3$ – x wt% Al_2O_3 (PPELA) Series

The specimen with 9 wt% of $LiCF_3SO_3$ salt of PPEL series shows the optimum amorphicity and ionic transport number as compared to the rest of the blend specimens. Hence, this specimen is selected as the base electrolyte for the preparation of next series wherein, Al_2O_3 nano-filler of various concentrations ranging from 2 wt% to 10 wt% is doped. This newly formed nano-composite PPELA series is given as '[$PVA_{(50)}$: $PEO_{(50)}$] – 6 wt% EC – 9 wt% $LiCF_3SO_3$ – x wt% Al_2O_3'. Various characteristic properties of these nano-composite blends are then studied in detail.

The XRD spectrum of PPELA series for varying amount of Al_2O_3 nano-filler is as depicted in Fig. 4.32. As observed from the figure, XRD scan of the specimen with 2 wt% of

Al_2O_3 shows a presence of a broad hump at ~ 14° corresponding to pure PVA and two intense peaks appearing at ~ 19° and ~ 23° corresponding to pure PEO. The intensities of these two peaks fluctuate with respect to the Al_2O_3 amounts in blend specimens. Also, two minor broad humps are observed at ~ 29° and ~ 40° for the specimens with Al_2O_3 = 2 wt% and 4 wt%. With the increasing amount of Al_2O_3 upto 6 wt%, these two humps suppress gradually, but with further addition of Al_2O_3, the hump again reappears and become quite visible at Al_2O_3 = 10 wt%.

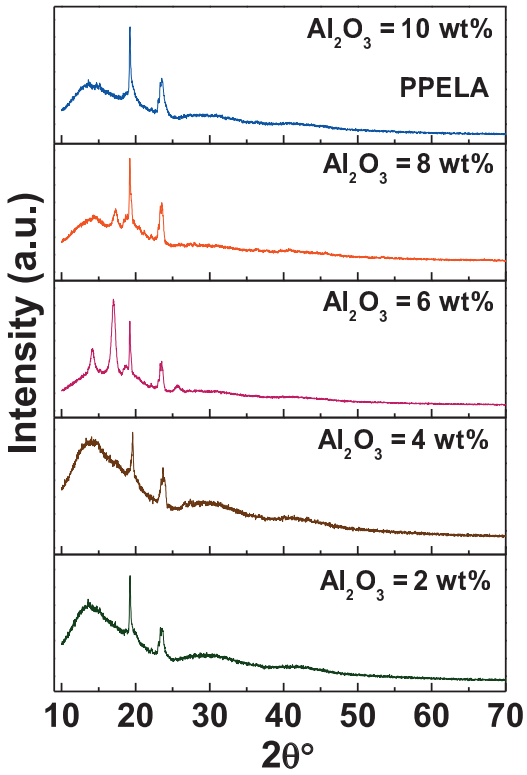

Fig. 4.32 XRD scans of blend specimens of PPELA series for varying Al_2O_3 amounts

Another interesting feature is seen at ~ 14°. Broad hump of PVA at ~ 14° gets gradually divided to form two sharp and intense peaks at ~ 14° and ~ 17° with substantial addition of nano-filler in blends. These features are prominently observed in XRD scan of the specimen with 6 wt% of Al_2O_3 . But with further addition of Al_2O_3 of 8 wt%, in blends, these two peaks start diminishing to reform the broad hump at ~ 14° as clearly visible from the XRD scan of the specimen with 10 wt% of Al_2O_3. Also, a small peak appears at ~ 26° in the

XRD scan of the specimen with Al_2O_3 = 6 wt% only. These observations suggest that with the incorporation of Al_2O_3 nano-filler beyond 6 wt% in blends, the amorphous phase in the blend matrix increases hence, reducing the crystallinity therein. The newly formed peaks and features in each XRD scan of the blends with the incorporation of Al_2O_3 nano-filler indicate the blend formation.

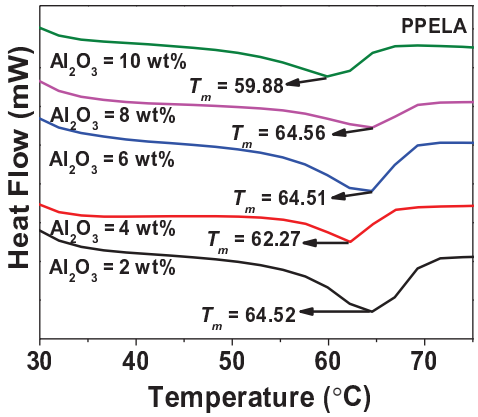

Fig. 4.33 DSC scans of blend specimens of PPELA series for varying Al_2O_3 amounts

Table 4.15 Variation in melting temperatures (T_m) and degree of crystallinity (X_c) of blend specimens of PPELA series for varying Al_2O_3 concentrations

Al_2O_3 *(wt%)*	Melting Temperature *(T_m)(°C)*	Degree of Crystallinity *(%X_c)*
2	64.52	76.31
4	62.27	81.22
6	64.51	90.12
8	64.56	60.51
10	59.88	50.18

DSC thermograms of the blend specimens of PPELA series as depicted in Fig. 4.33 show the presence of a single endothermic peak which corresponds to the melting of PEO in the respective blend specimen. As the content of nano-filler increases, these melting peaks show a shifting which indicates the compatibility and miscibility amongst PVA and PEO host polymers [51]. The melting temperatures 'T_m' of the blends of PPELA series which lie in the temperature range of 59 °C to 65 °C are shown in Table 4.15. The table provides the values of degree of crystallinity 'X_c' also which increase gradually with the initial increase of the Al_2O_3 nano-filler content upto 6 wt% in blends but substantially drop down with its further addition. The increment in 'X_c' values at initial levels of Al_2O_3 nano-filler means the reduction in amorphicity or the increase in the stiffness of polymeric chains. But after 6 wt%, the dispersion of Al_2O_3 reverses the trend and the chain stiffness reduces. Consequently, the 'X_c' values drop down.

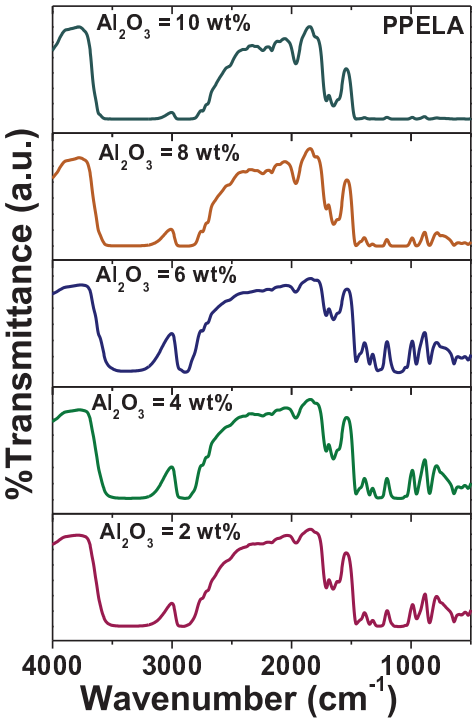

Fig. 4.34 FT-IR spectra of blend specimens of PPELA series for varying Al_2O_3 contents

Table 4.16 Vibrational modes & wavenumbers exhibited by the blend specimens of PPELA series for varying Al_2O_3 contents

Wavenumber (cm^{-1})	Assignment
3550-3100	Intermolecular OH Stretching (hydroxyl) band of PVA: characteristic feature of alcohols
2935-2800	C–H stretching of PEO
2241	C–H Stretching of PEO/ C=O Combination of PEO
2165	Asymmetric C–H Stretching of PEO/ C–H Deformation Combination of PEO
1962	Asymmetric Stretching Band of PEO
1724	C=O Stretching of PVA
1647	C=C Stretching of PVA
1466	CH_2 Scissoring of PEO
1348	CH_2 Wagging of PEO
1280	Asymmetric CH_2 Twisting of PEO
1104	C-O-C Stretching of PEO
950	CH_2 Symmetric Rocking of PEO/ C–O–C Asymmetric Stretching of PEO
842	CH_2 Twisting of PEO/ CH_2 Wagging of PEO
640	OH Twisting of PVA
528	C-O-C Bending of PEO

The FT-IR spectra of blends of PPELA series at different concentrations of Al_2O_3 nano-filler have been depicted in Fig. 4.34 and the assignments of various bands have been respectively, listed in Table 4.16. Broad bands appearing in approximate range of 3550 cm^{-1} to 3100 cm^{-1} and 2935 cm^{-1} to 2800 cm^{-1} in FT-IR spectrum of blend specimen with 2 wt% of Al_2O_3, gradually narrows down with increasing content of Al_2O_3 upto 6 wt%. Moreover, the features observed in the range of 1500 cm^{-1} to 500 cm^{-1}, get slightly intense with respect to Al_2O_3 concentrations at initial levels. But with further increment of Al_2O_3 nano-filler in blends beyond 6 wt%, the broad bands observed in the range of approximately 3550 cm^{-1} to 2800 cm^{-1}, get significantly broader. Also, most of the features at 1500 cm^{-1} to 500 cm^{-1} suppress gradually and almost disappear in FT-IR spectrum of blend with Al_2O_3 = 10 wt%. This however, suggests the increase in amorphicity of the blend matrix. Actually, in this case,

the chain stiffness decreases which reduces the peak intensity showing as if the system is continuously getting amorphous. But this phenomenon takes place at higher concentrations of Al_2O_3 nano-filler beyond 6 wt% in the blends.

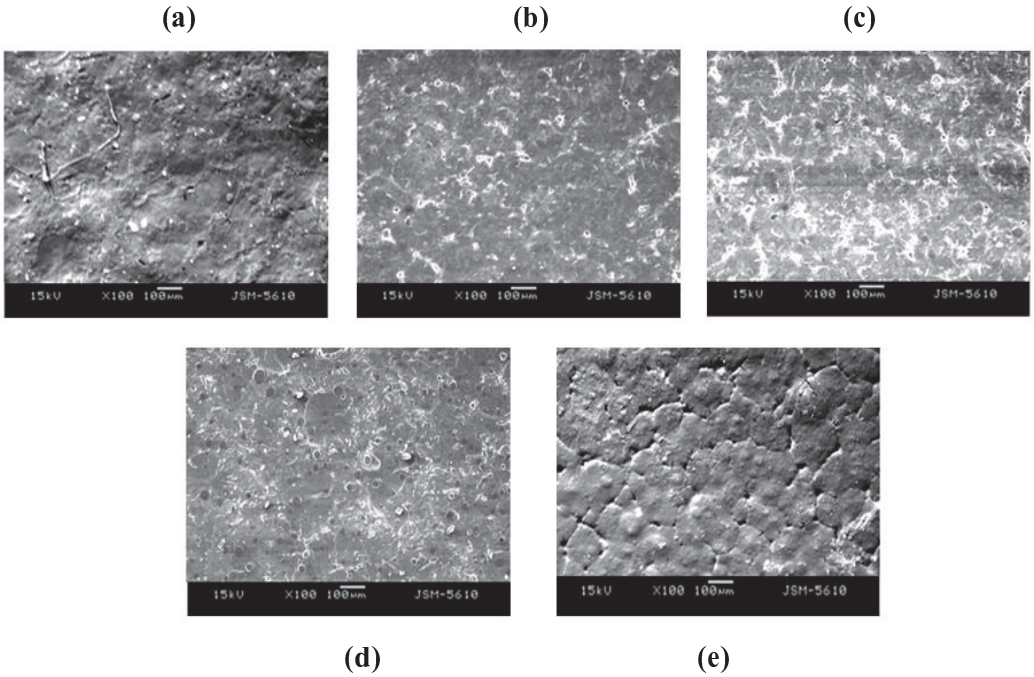

Fig. 4.35 SEM images of blend specimens of PPELA series for (a) Al_2O_3 = 2 wt%, (b) Al_2O_3 = 4 wt%, (c) Al_2O_3 = 6 wt%, (d) Al_2O_3 = 8 wt% and (e) Al_2O_3 = 10 wt%

SEM micrographs of these blends for varying concentrations of Al_2O_3 are depicted in Fig. 4.35 (a) to (e). The SEM image of the blend specimen with 2 wt% of Al_2O_3 shows presence of small white spots and patches along with a very few number of black spots or pores. These white spots and patches increase gradually upto 6 wt% of Al_2O_3 in blends. But with further addition of Al_2O_3 upto 10 wt%, black pores increase significantly; while the white spots and patches are reduced or hardly seen. This shows the homogeneous distribution of nano-filler particles dispersed in the electrolyte film at Al_2O_3 > 6 wt%. Surface roughness at $Al_2O_3 \leq 6$ wt% is associated with high surface free energy. On the other hand, improvement in the smoothness of the blend surfaces with respect to Al_2O_3 content > 6 wt% relates to the reduction in the crystalline phases of the polymer electrolyte film. Hence, smoothening of blend surface at Al_2O_3 beyond 6 wt% indicates reduction in the stiffness of

polymeric chains of the electrolytes owing to which conductivity may enhance as discussed in the later chapter.

Fig. 4.36 shows variation of ionic transport number 't_i' against increasing Al_2O_3 nano-filler content in the polymer matrix. The 't_i' value decreases initially with the increase in Al_2O_3 content in blends upto 6 wt% and afterwards starts increasing upto its 10 wt% therein. At low amount of Al_2O_3, the ionic transport number values are low and continue to drop with gradual incorporation of nano-filler in the blend specimens. This means that solvation of salt is low and decreases continuously with further addition of Al_2O_3 in the blend matrices. Moreover, at low nano-filler concentrations upto 6 wt%, nano-filler particles are expected to come together forming neutral aggregates and blocking the conducing pathways which result in the increase in the crystallinity of blend matrix and reduction in its amorphicity and flexibility hence, hindering the movement of Li^+ and $CF_3SO_3^-$ along with polymeric chain segments through blend matrices via conducting pathways.

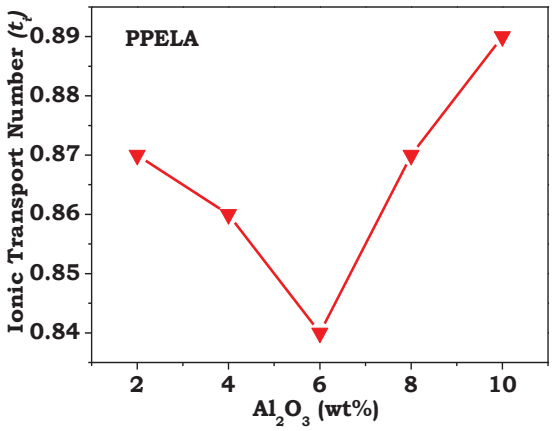

Fig. 4.36 Variation in ionic transport number (t_i) of blend specimens of PPELA series for different Al_2O_3 concentrations

However, at higher concentrations of Al_2O_3 > 6 wt%, random distribution of nano-filler particles initiates the formation of free volume in the blend matrix. This in turn increases the amorphicity in the blend matrix, imparts flexibility to it and avails conducting pathways for the transport of free Li^+ and $CF_3SO_3^-$ and segments of polymeric chains through this matrix.

These results are in excellent confirmation with the dc conductivity with respect to Al_2O_3 concentrations in the blends, as also discussed in the next chapter.

4.8 $LiMn_2O_4$ Cathode Material

Fig. 4.37 shows the XRD spectrum of $LiMn_2O_4$ powder wherein, the peaks are present at about 18°, 36°, 37°, 43°, 48°, 58°, 63° and 67°. The presence of these peaks confirms the formation of a single phased cubic spinel structure of $LiMn_2O_4$ with the space group of Fd3m and indicates the spinel $LiMn_2O_4$ as the main phase. No notable formation of secondary phases or impurities is observed [74]. FT-IR spectrum of $LiMn_2O_4$ powder, as shown in the Fig. 4.38 shows presence of two important transmittance peaks at 615 cm^{-1} and 515 cm^{-1}.

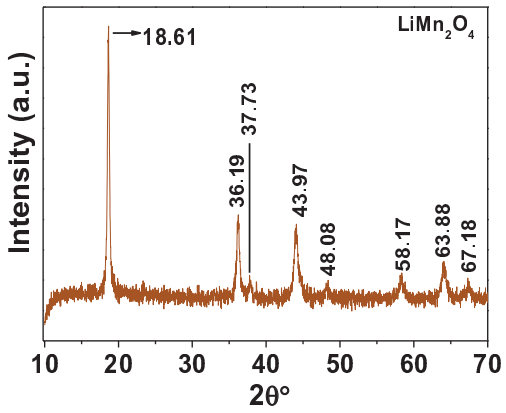

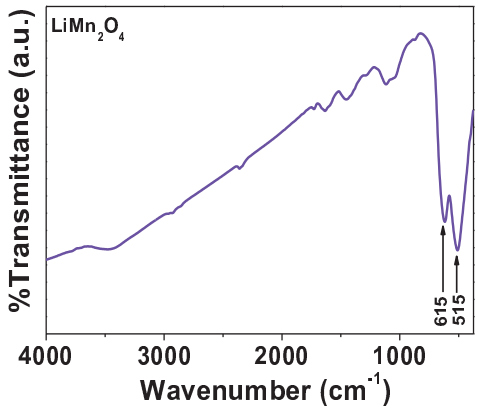

Fig. 4.37 XRD spectrum of $LiMn_2O_4$ powder **Fig. 4.38** FT-IR spectrum of $LiMn_2O_4$ powder

The peak at 615 cm^{-1} corresponds to the Mn-O stretching vibration of the MnO_6 octahedron whereas, the one at 515 cm^{-1} is assigned to the metal–oxygen vibrations in LiO_6 tetrahedrons, basically attributed to the Li-O bending vibrations. Hence, these two absorption peaks at 615 cm^{-1} and 515 cm^{-1} refer to stretching vibration of Mn(III)-O and Mn(IV)-O bonds, respectively [75-78]. Both these XRD and FT-IR studies of $LiMn_2O_4$ powder confirm its structure to be *'Spinel'* in nature.

References

[1] I.S. Elashmawi, N.A. Hakeem, E.M. Abdelrazek, *Physica B* 403 (2008) 3547.

[2] Z. Osman, K.B.M. Isa, A. Ahmad, L. Othman, *Ionics* 16 (2010) 431.

[3] C.W. Liew, Y.S. Ong, J.Y. Lim, C.S. Lim, K.H. Teoh, S. Ramesh, *Int. J. Electrochem. Sci.* 8 (2013) 7779.

[4] P. Joge, D.K. Kanchan, P. Sharma, M. Jayswal, D.K. Avasthi, *Radiation Physics and Chemistry* 100 (2014) 74.

[5] S.K. Chaurasia, A. Chandra, *Solid State Ionics* 307 (2017) 35.

[6] S. Klongkan, J. Pumchusak, *Electrochimica Acta* 161 (2015) 171.

[7] R. Nadimicherla, R. Kalla, R. Muchakayala, X. Guo, *Solid State Ionics* 278 (2015) 260.

[8] P. Sharma, D.K. Kanchan, *Ionics* 19 (2013) 1285.

[9] K. Merrett, R.M. Cornelius, W.G. Mcclung, L.D. Unsworth, H. Sheardown, *J. Biomater. Sci. Polymer Edn.* 13 (2002) 593.

[10] S. Zhang, J.Y. Lee, L. Hong, *J. Power Sources* 126 (2004) 125.

[11] I.I. Olsen, R. Koksbang, E. Skou, *Electrochimica Acta* 40 (11) (1995) 1701.

[12] M. Ciosek, M. Siekierski, W. Wieczorek, *Electrochimica Acta* 50 (2005) 3922.

[13] P. Pradeepa, S.E. Raj, G. Sowmya, J. Kalaiselvimary, M.R. Prabhu, *Materials Science and Engineering B* 205 (2016) 6.

[14] B.K. Money, K. Hariharan, *Appl. Phys. A* 88 (2007) 647.

[15] S.K. Chaurasia, R.K. Singh, S. Chandra, *Solid State Ionics* 183 (2011) 32.

[16] T.J.R. Reddy, V.B.S. Achari, A.K. Sharma, V.V.R.N. Rao, *Ionics* 13 (2007) 55.

[17] T. Sreekanth, M.J. Reddy, S. Ramalingaiah, U.V.S. Rao, *J. Power Sources* 79 (1999) 105.

[18] D.K. Pradhan, B.K. Samantaray, R.N.P. Choudhary, A.K. Thakur, *Ionics* 11 (2005) 95.

[19] M.R. Johan, L.B. Fen, *Ionics* 16 (2010) 335.

[20] S.L. Agrawal, M. Singh, M. Tripathi, M.M. Dwivedi, K. Pandey, *J. Mater. Sci.* 44 (2009) 6060.

[21] P. Joge, D.K. Kanchan, P. Sharma, N. Gondaliya, *Indian Journal of Pure & Applied Physics* 51 (2013) 350.

[22] S. Ramesh, T.F. Yuen, C.J. Shen, *Spectrochimica Acta Part A* 69 (2008) 670.

[23] E.M. Abdelrazek, I.S. Elashmawi, S. Labeeb, *Physica B* 405 (2010) 2021.

[24] M. Sundar, S. Selladurai, *Ionics* 12 (2006) 281.

[25] Z. Osman, N.M. Ansor, K.W. Chew, N. Kamarulzaman, *Ionics* 11 (2005) 431.

[26] P.B. Bhargav, V.M. Mohan, A.K. Sharma, V.V.R.N. Rao, *Ionics* 13 (2007) 173.

[27] G. Hirankumar, S. Selvasekarapandian, M.S. Bhuvaneswari, R. Baskaran, M. Vijayakumar, *J. Solid State Electrochem.* 10 (2006) 193.

[28] S. Chintapalli, C. Zea, R. Frech, *Solid State Ionics* 92 (1996) 205.

[29] A. Hashmi, A. Kumar, K.K. Maurya, S. Chandra, *J. Phys. D: Appl. Phys.* 23 (1990) 1307.

[30] P.B. Bhargav, V.M. Mohan, A.K. Sharma, V.V.R.N. Rao, *Ionics* 13 (2007) 441.

[31] S. Ibrahim, M.M. Yassin, R. Ahmad, M.R. Johan, *Ionics* 17 (2011) 399.

[32] K. Kulasekarapandian, S. Jayanthi, A. Muthukumari, A. Arulsankar, B. Sundaresan, *International Journal of Engineering Research and Development* 5 (11) (2013) 30.

[33] W. Tan, *International Journal of the Institute of Materials Malaysia* 1 (2013) 125.

[34] S. Ramesh, L.J. Yi, *Ionics* 15 (2009) 413.

[35] S. Ramesh, L.C. Wen, *Ionics* 16 (2010) 255.

[36] S. Ramesh, M.F. Chai, *Materials Science and Engineering B* 139 (2007) 240.

[37] R. Sathyamoorthy, S. Velumani, A. Subbarayan, K. Natarajan, P.J. Sebastian, *J. New. Mat. Electrochem. Systems* 8 (2005) 121.

[38] M.R. Johan, O.H. Shy, S. Ibrahim, S.M.M. Yassin, T.Y. Hui, *Solid State Ionics* 196 (2011) 41.

[39] P. Prabakaran, R.P. Manimuthu, S. Gurusamy, E. Sebasthiyan, *Chinese Journal of Polymer Science* 35 (3) (2017) 407.

[40] C.A. Finch. *Stereochemistry of Polyvinyl Alcohol. Polyvinyl Alcohol: Properties and Applications,* A Wiley-Interscience Publication, England, 1973, pp. 203.

[41] N. Gondaliya, *Ph.D. Thesis*, Department of Physics, The M.S. University of Baroda, Vadodara, 2013.

[42] M.A.A. Mendez, E.S.M. Martinez, L.O. Arroyo, G.C. Portillo, E.S. Espindola, *J. Nanopart. Res.* 13 (2011) 2525.

[43] J.W. Cho, J.H. So, *Mater. Lett.* 60 (2006) 2653.

[44] P. Sharma, *Ph.D. Thesis*, Department of Physics, The M.S. University of Baroda, 2013.

[45] O.G. Abdullah, S.B. Aziz, M.A. Rasheed, *Results in Physics* 6 (2016) 1103.

[46] A. Das, A.K. Thakur, K. Kumar, *Solid State Ionics* 262 (2014) 815.

[47] M. Ulaganathan, S. Rajendran, *Ionics* 16 (2010) 515.

[48] R.J. Sengwa, P. Dhatarwal, S. Choudhary, *Electrochimica Acta* 142 (2014) 359.

[49] R.M. Hodge, G.H. Edward, G.P. Simon, *Polymer* 37 (1996) 1371–1376.

[50] P. Sharma, D.K. Kanchan, N. Gondaliya, M. Pant, M.S. Jayswal, *Ionics* 19 (2013) 301.

[51] P. Joge, D.K. Kanchan, P. Sharma, N. Gondaliya, *Advanced Materials Research* 665 (2013) 227.

[52] S.R. Sudhamani, M.S. Prasad, K.U. Sankar, *Food Hydrocoll.* 17 (2003) 245.

[53] J. Lee, D. Bhattacharyya, A.J. Easteal, J.B. Metson, *Current Appl. Phys.* 8 (2008) 42.

[54] R.A. Senthil, J. Theerthagiri, J. Madhavan, A.K. Arof, *Optical Materials* 58 (2016) 357.

[55] E. Aram, M. Ehsani, H.A. Khonakdar, *Thermochimica Acta* 615 (2015)61.

[56] H. Sun, C. Ma. T. Wang, Y. Xu, B. Yuan, Y. Kong, *Materials Chemistry and Physics* 148 (2014) 790.

[57] P. Sharma, D.K. Kanchan, N. Gondaliya, M. Jayswal, P. Joge, *Indian Journal of Pure & Applied Physics* 51 (2013) 346.

[58] H.H. Sumathipala, J. Hassoun, S. Panero, B. Scrosati, *Ionics* 13 (2007) 281.

[59] S. Sultana, R. Rafiuddin, *Ionics* 15 (2009) 621.

[60] A. Chandra, A. Chandra, K. Thakur, *Arabian Journal of Chemistry* 9 (2016) 400.

[61] W. Zhai, Y.W. Zhang, L. Wang, F. Ca, X.M. Liu, Y.J. Shi, H. Yang, *Solid State Ionics* 286 (2016) 111.

[62] S. Ketabi, K. Lian, *Electrochimica Acta* 154 (2015) 404.

[63] K. Mishra, S. Singh Pundir, D.K. Rai, *Ionics* 23 (2017)105.

[64] H.J. Woo, A.K. Arof, *Spectrochimica Acta Part A: Molecular and Biomolecular Spectroscopy* 161 (2016) 44.

[65] R. Muchakayala, S. Song, S. Gao, X. Wang, Y. Fan, *Polymer Testing* 58 (2017) 116.

[66] P. Sharma, D.K. Kanchan, N. Gondaliya, *Ionics* 19 (2013) 777.

[67] A.L. Saroj, R.K. Singh, S. Chandra, *Journal of Physics and Chemistry of Solids* 75 (2014) 849.

[68] M. Ravi, K.K. Kumar, V.M. Mohan, V.V.R.N. Rao, *Polymer Testing* 33 (2014) 152.

[69] K. Kesavan, C.M. Mathew, S. Rajendran, M. Ulaganathan, *Materials Science and Engineering B* 184 (2014) 26.

[70] A. Kumar, R. Sharma, M.K. Das, P. Gajbhiye, K.K. Kar, *Electrochimica Acta* 215 (2016) 1.

[71] M. Muthuvinayagam, C. Gopinathan, *Polymer* 68 (2015) 122.

[72] D.V. Pandi, S. Selvasekarapandian, R. Bhuvaneswari, M. Premalatha, S. Monisha, D. Arunkumar, K. Junichi, *Solid State Ionics* 298 (2016) 15.

[73] Y.L. Ni'mah, M.Y. Cheng, J.H. Cheng, J. Rick, B.J. Hwang, *Journal of Power Sources* 278 (2015) 375.

[74] X. Zhou, M. Chen, H. Bai, J. Guo, *Vacuum* 99 (2014) 49.

[75] P. Cui, Y. Liang, *Solid State Ionics* 249-250 (2013) 129.

[76] S. Jayapal, R. Mariappan, S. Sundar, S. Piraman, *Journal of Electroanalytical Chemistry* 720-721 (2014) 58.

[77] S. Zhao, Y. Bai, L. Ding, B. Wang, W. Zhang, *Solid State Ionics* 247-248 (2013) 22.

[78] X. Li, Y. Xu, *Applied Surface Science* 253 (2007) 8592.